(REVISION 2) Thermodynamics, self-diffusion, and structure of liquid $NaAlSi_3O_8$ to 30 GPa by classical molecular dynamics simulations

Ryan T. Neilson[1], Frank J. Spera[1], and Mark S. Ghiorso[2]

[1]Department of Earth Science, University of California-Santa Barbara, Webb Hall 1006—MC 9630, Santa Barbara, California 93106, U.S.A.

[2]OFM Research, 7336 24th Avenue NE, Seattle, Washington 98115, U.S.A.

Abstract

Understanding the thermodynamics of liquid silicates at high pressure and temperature is essential for many petrologic problems, and sodium aluminosilicates are an important component of most magmatic systems. We provide a high-pressure equation of state (EOS) for liquid $NaAlSi_3O_8$ based upon molecular dynamics (MD) simulations. The resulting thermodynamic properties have changes in pressure and temperature correlative to trends in diffusion and atomic structure, giving insight to the connections between macroscopic and microscopic properties. Internal pressure shows a maximum in attractive inter-atomic forces at low pressure, giving way to the dominance of repulsive forces at higher pressure. Self-diffusion coefficients (D) typically order $D_{Na} > D_{Al} > D_O > D_{Si}$. At the lowest temperature, self-diffusivity (anomalously) increases as pressure increases up to ~5–6 GPa for Al, Si, and O. Diffusion data outside this "anomalous" region are fit by a modified Arrhenius expression, from which activation energies are calculated: 85 kJ/mol (Na) to 140 kJ/mol (Si). The amount of AlO_4 and SiO_4 polyhedra (tetrahedra) decreases upon compression and is approximately inversely-correlated to the abundance of 5- and 6-fold structures. Average coordination numbers for Al-O, O-O, and Na-O polyhedra increase sharply at low pressure but start to stabilize at higher pressure, corresponding to changes in inter-atomic repulsion forces as measured by the internal pressure. High-pressure repulsion also correlates with a close-packed O-O structure where ~12 O atoms surround a central O. Self-diffusivity stabilizes at higher pressures as well. Relationships between the internal pressure,

self-diffusion, and structural properties illustrate the link between thermodynamic, transport, and structural properties of liquid $NaAlSi_3O_8$ at high pressure and temperature, shedding light on how microscopic structural changes influence macroscopic properties in molten aluminosilicates.

Keywords

Thermodynamics, molecular dynamics, melt, $NaAlSi_3O_8$, equation of state, self-diffusion, coordination number, internal pressure, liquid structure

Introduction

Thermodynamic and transport properties of liquid silicates at high pressure (*P*) and temperature (*T*) play fundamental roles in petrologic systems, such as magmatic processes, mantle dynamics, phase transitions, and planetary differentiation. For example, heat capacity plays an important role in estimating the total heat flux of Earth (Stacey 1995; Lay et al. 2008). The fundamental nature of these material properties may be explained by an appeal to the atomic structure of the melt. Understanding the relationship between short-range liquid structure (atomic arrangement) and thermodynamics illuminates the underlying microscopic controls on macroscopic properties of silicate liquids.

Classical molecular dynamics (MD) simulations have enabled geologists and geophysicists to explore thermodynamic properties of liquid silicates at *P* and *T* conditions beyond those accessible in the laboratory. Since the work of Woodcock et al. (1976), high-*T* and high-*P* thermodynamic properties, self-diffusion, and melt structure have been studied for various compositions using classical MD simulations (e.g., Angell et al. 1982; Bryce et al. 1999; Oganov et al. 2000; Saika-Voivod et al. 2000; Ghiorso 2004a; Lacks et al. 2007; Spera et al. 2011; Creamer 2012). Because the position of all ions are known during MD simulation, the structural arrangement of atoms can be "observed" concomitantly with the *P*- and *T*-

dependencies of thermodynamic and transport properties. While laboratory experiments provide standards for material properties, only MD simulations can fully explore the connection between the structure and thermodynamics of silicate melts at extreme P (> 10 GPa) and T (> 2000 K). Recent computational advancements and improvements in the pair-potential parameters strengthen the statistical mechanics of MD calculations, offering greater precision and accuracy to thermodynamic models. Although investigated by MD simulations in previous decades (e.g., Stein and Spera 1995, 1996; Bryce et al. 1999), liquid $NaAlSi_3O_8$ (albite composition) has not been explored in the detail currently available for classical MD simulations.

In the present work, an equation of state (EOS) for liquid $NaAlSi_3O_8$ is developed for the P-T range 0–30 GPa and 3100–5100 K from classical MD simulations with the effective pair-potential of Matsui (1998). A table summary of the MD results is given in Electronic Appendix 1 (EA-1). Results were fit to an EOS based on the Universal Equation of State of Vinet et al. (1986, 1987, 1989) and an energy-scaling relationship developed by Rosenfeld and Tarazona (1998) (described in next section). Thermodynamic properties, calculated from the EOS using standard identities, are tabulated by P and T in Electronic Appendix 2 (EA-2).

We present the MD results of $NaAlSi_3O_8$ melt and discuss their import under three main headings: Thermodynamics, Self-diffusion, and Structure. Results are compared to available experimental data. The internal energy (E), isochoric heat capacity (C_V), thermal pressure coefficient, coefficient of thermal expansion (i.e., expansivity, α), and isothermal compressibility (β_T) are discussed in the Thermodynamics section. Internal pressure, an important thermodynamic property relating cohesive forces acting on the liquid structure, is discussed separately. Coefficients of self-diffusion (D) were analyzed with respect to thermodynamic properties and are presented in the Self-diffusion section. A modified Arrhenius model for all D

values is also given. In the Structure section, the coordination statistics of the liquid structure are discussed and then synthesized in relation to thermodynamics and self-diffusion. Tables of *D* values and coordination statistics are provided in EA-1. Mild changes in liquid structure at high *P* correspond to patterns expressed in the thermodynamic and transport properties of $NaAlSi_3O_8$, suggesting a stabilizing relationship between atomic arrangement, mobility, and macroscopic properties.

Theory and Calculations

Pair-potential parameters and MD calculations

Classical MD simulations utilize empirical pair-potential parameters designed for the specific composition and bond types of the system. Matsui (1998) developed a set of pair-potential parameters for the NaO_2-CaO-MgO-Al_2O_3-SiO_2 (NCMAS) system as a transferrable ionic potential model. Thermodynamic data from 29 crystals and five liquids (including liquid $NaAlSi_3O_8$) in the NCMAS system were used to empirically fit the parameters, and MD simulations of these crystal and liquid compositions "compared well with the available experimental data" (Matsui 1998, p. 145).

MD results based on the Matsui (1998) parameters have shown good comparison with experimental measurements (Martin et al. 2009) and with results of other pair-potential sets (Spera et al. 2011) up to ~30 GPa at high *T*. As the empirical fits were based on abundant mineral data, the potential of Matsui (1998) is considerably more reliable than older sets based on fewer data. Results for $NaAlSi_3O_8$ in Bryce et al. (1999) were calculated from an older potential, a smaller range of *T*, fewer particles in the ensemble, and about one-tenth of the number of simulations as the present work. Additionally, the ubiquity of the NCMAS system in planet Earth adds to the value of the Matsui (1998) potential for modeling petrologic systems.

Of course, the validity of any model should be assessed against laboratory data. Our results are compared with experimental data, although extrapolations in *P* and *T* are required. Laboratory studies on liquid $NaAlSi_3O_8$ have generally focused on the range 900–2100 K and 1 bar to 12 GPa (Kushiro 1978; Stebbins et al. 1982, 1983; Richet and Bottinga 1980, 1984; Stein et al. 1986; Kress et al. 1988; Lange 1996; Poe et al. 1997; Anovitz and Blencoe 1999; Tenner et al. 2007; Gaudio et al. 2015). It is also important to consider the *T* range over which the experiments were performed. Relatively large errors in the *T*- (or *P*-) extrapolation of certain properties (e.g., *D*) can occur if the range in *T* (or *P*) over which the property was measured is small—a case not uncommon to diffusion experiments.

The large extrapolation in *T* between experiments and MD simulations is principally due to the high glass transition temperature (T_g) at fast cooling (quench) rates. Because of the rapid quench rate used in our MD simulations, *T* was kept above 3000 K for all results to avoid intercepting non-ergodic (non-equilibrium) behavior below T_g. As quench rates in MD simulations are about 10^{14} K/s—around 14 orders of magnitude larger than typical laboratory cooling rates—the computer T_g is higher than the laboratory T_g. For $NaAlSi_3O_8$, the T_g at laboratory cooling rates is 1036 K (Arndt and Häberle 1973). Other experiments estimate T_g for $NaAlSi_3O_8$ at 1050, 1130, and 1223 K with cooling rates 0.33, 33.3, and 3333 K/s, respectively (Richet and Bottinga 1986). MD simulations in the range 2000–3000 K (Neilson unpublished data) indicate that the computer T_g for $NaAlSi_3O_8$ may be close to 3000 K at 1 bar with a slight dependence on *P*. Hence, in order to compare MD results with laboratory studies, we are forced to extrapolate the ergodic (equilibrium) liquid properties to the supercooled metastable state. Observing the quality of the EOS fit, we believe this extrapolation is reasonably robust.

EOS development

An EOS for liquid $NaAlSi_3O_8$ was developed by fitting MD results to the Universal EOS of Vinet et al. (1986, 1987, 1989). The Universal EOS of solids (Vinet et al. 1986) is based on fundamental atomic interactions and, consequently, generally applies to all classes of solids and to liquids at high P (e.g., Ghiorso 2004b; Ghiorso et al. 2009). While many types of EOS exist, the simplicity of the Universal EOS and its applicability at high P give flexibility to the analysis. The result of the Universal EOS fit was then used in conjunction with the energy-scaling relationship of Rosenfeld and Tarazona (1998) to develop a thermodynamic EOS with the form:

$$- \qquad (1)$$

where E_p and E_k are potential and kinetic energy, respectively. Terms $a(V)$ and $b(V)$ are solely functions of volume (V) fitted empirically from the simulations, R is the universal gas constant, and n is the number of atoms per formula unit (e.g., $n = 13$ for $NaAlSi_3O_8$). Equation 1 includes the thermodynamic expression $E_p = a(V) + b(V)T^{3/5}$ developed by Rosenfeld and Tarazona (1998) for dense fluids (see next paragraph). The last term on the right hand side of Equation 1 represents the classical high-T limit for E_k. Agreement between the classical E_k limit and the MD results is excellent (see EA-1).

Rosenfeld and Tarazona (1998) developed an analytical model for dense solids and fluids based on thermodynamic perturbation theory, using a fundamental-measure reference functional for hard spheres with an expansion of the free energy. With reference system parameters chosen via variational perturbation theory, the free energy functional captures the true divergence of an EOS for continuous (soft) interactions at close-packing configurations and provides the entire density profile across the singularity. The resulting variational perturbation functional, which posits that the Madelung (potential) energy scales with $T^{3/5}$, generally applies to all pair potentials, and comparison with simulation results (with various forms of the potential) yields

accurate predictions of equations of state (Rosenfeld and Tarazona 1998). In addition to being theoretically sound, the fundamental-measure functional provides a "physically acceptable free energy model" of an "ideal liquid" (Rosenfeld and Tarazona 1998, p. 149) and well describes thermodynamic properties of solids and liquids at high density.

Multiple studies have confirmed the Rosenfeld and Tarazona (1998) model for a variety of liquids with different types of bonding (Sastry 2000; Coluzzi and Verrocchio 2002; Ingebrigtsen et al. 2013). The $T^{3/5}$ scaling has been demonstrated for high-T silicate melt with several compositions (Saika-Voivod et al. 2000; Martin et al. 2009; Ghiorso et al. 2009; Spera et al. 2011; Creamer 2012; Martin et al. 2012). Multiple MD simulation studies have combined the $T^{3/5}$ scaling relationship with the Universal EOS of Vinet et al. (1986, 1987, 1989) to develop an EOS for silicate liquids (Ghiorso et al. 2009; Martin et al. 2009). We find this methodology to be self-consistent and applicable to a large range of compositions on Earth.

The MD results of the present study fit the $T^{3/5}$ scaling relationship with coefficients of determination (R^2) $\geq$ 0.999 for each isochore. Fitting $a(V)$ and $b(V)$ parameters over all isochores yielded R^2 values of 0.9975 and 0.9983, respectively. Following the work of Saika-Voivod et al. (2000), we derived $P(V,T)$ from Equation 1 using standard thermodynamic identities. This procedure is described elsewhere (Ghiorso et al. 2009). Based on the strength of the fit for $a(V)$ and $b(V)$, in addition to the agreement between the MD results and the classical E_k limit, the developed EOS appears to faithfully capture the thermodynamic properties of liquid $NaAlSi_3O_8$ over the range 3100–5100 K and 0–30 GPa.

Internal pressure and inter-atomic forces

An informative way to investigate intermolecular (or inter-atomic) forces in a liquid is to examine the internal pressure (P_{int}). Qualitatively, P_{int} is a measure of the cohesive forces within

a fluid. Molten $NaAlSi_3O_8$, for example, is herein modeled with long-range Coulombic forces (attractive and repulsive), short-range Born electron repulsive forces, and van der Waals attractive forces. The net contribution of these forces can be related to P_{int}.

Differentiating the fundamental equation of thermodynamics with respect to V at constant T yields $(\partial E/\partial V)_T = T(\partial S/\partial V)_T - P$. Applying Maxwell's relation $(\partial S/\partial V)_T = (\partial P/\partial T)_V$ produces the thermodynamic definition of internal pressure:

— — — . (2)

Following the cogent arguments of Kartsev et al. (2012), P_{int} is created by repulsive and attractive forces acting on the structural components of a liquid, which forces are related to the E_p gradient over V. Thus, the internal pressure can be expressed in terms of the inter-atomic forces (F) according to

— —— —— — (3)

where contributions from net repulsive and net attractive forces are indicated by *rep* and *att*, respectively (Kartsev 2004; Kartsev et al. 2012). Note the definition of a new quantity, P_{int}^{F} {Note to typesetting: the "*F*" and "*int*" are to be stacked} (cf. Equation 2). The sign convention is adopted so that repulsive forces are considered positive and attractive forces are negative. Therefore, the respective components of the internal pressure are positive and negative (i.e., $P_{int}^{rep} > 0$ and $P_{int}^{att} < 0$) {Note to typesetting: "*rep*" and "*att*" are to be stacked above "*int*" on the respective symbol}. When $|P_{int}^{att}| > P_{int}^{rep}$, attractive forces dominate the internal force field of the liquid, and P_{int}^{F} is negative (Kartsev et al. 2012). Because P_{int}^{F} bears a strong relationship to liquid structure, the influence of inter-atomic forces on atomic arrangement can be qualitatively determined from fundamental thermodynamic properties.

Method

Details of the classical MD method are well described in the literature (e.g., Allen and Tildesley 1987; Rapaport 1995). The potential used in this work is an effective pair-potential function of distance (r_{ij}) between atoms i and j:

$$\text{———} \qquad \text{—} \qquad \text{—}. \tag{4}$$

The empirical pair-wise constants A_{ij} and C_{ij} are energy scalars for electron repulsion and van der Waals attractive forces, respectively. B_{ij} characterizes the decay of electron repulsion energy between atoms i and j; ε_0 is the vacuum permittivity; q_i is the charge on atom i; and e is the electronic charge. Equation 4 incorporates Coulombic forces, Born electrostatic repulsion, and van der Waals attractive forces (Matsui 1998; Cygan 2001; Spera et al. 2009, 2011).

One hundred fifty-two classical MD simulations were performed for liquid $NaAlSi_3O_8$ with density (ρ) between 1.8 and 3.6 g/cm^3. For a given ρ, eight target temperatures were spaced every 300 K from 3000 to 5100 K (Figure 1). All simulations were performed with the Large-scale Atomic/Molecular Massively Parallel Simulator (LAMMPS) code, using the Verlet algorithm with 1 fs time steps (Plimpton 1995). The pair-potential parameters of Matsui (1998) used in Equation 4 are listed in Table 1. Short- and long-range forces were calculated using the Particle-Particle Particle-Mesh method (Hockney and Eastwood 1988), with a radial cut-off length of 11 Å. Resulting P ranged from -0.41 to 42.21 GPa (EA-1). Simulations were carried out in the microcanonical ensemble: holding constant E, V, and the number of particles (N). Every simulation had 13,000 particles (1,000 formula units of $NaAlSi_3O_8$), and cell volumes varied between 1.2×10^5 and 1.9×10^5 Å^3.

Initial conditions for atom positions and velocities were randomly generated using a skew start algorithm and an initial T of 10,000 K (cf. Refson 2001; Nevins and Spera 2007; Nevins 2009). The system was held at 10,000 K for ~25 ps and then rapidly cooled (quenched) by

velocity scaling to the target T at a constant rate of ~100 K/ps. Once at the target T, an additional 3–5 ps simulation time was given to allow for equilibration. Immediately thereafter, the production stage began and continued for 50 ps. A student t-test was conducted on P and T values from the 50 ps production step to determine if thermal equilibrium was attained. If thermal equilibrium was not reached, time was added to the pre-production stage, and the simulation was performed again. All conclusions for this work are based upon simulations that maintained thermal equilibrium during the production step. Average values for P, T, E, E_k, E_p, as well as the statistical fluctuations (σ) for P and T, were calculated from the results of the 50 ps production step and are provided in EA-1.

Self-diffusivity (i.e., D) was calculated from the mean-square displacement of each atom type during the simulation production step. The Einstein expression

— (5)

relates D to the averaged square displacement of N particles over time (t) (Rapaport 1995). D values for Na, Al, Si, and O are listed by P and T in EA-1. All diffusivities from the MD results were fit to a modified Arrhenius expression (Equation 7), yielding activation energies and volumes (discussed in the Self-diffusion section).

Short-range liquid structure was determined by coordination statistics—compiled in EA-1. Coordination numbers (CN) were counted for every pairing arrangement with O (e.g., Na-O, Si-O, O-Si, O-O). These counts were summed and binned according to CN to calculate the fractional distribution of all pair-specific polyhedra. Nearest-neighbor counts were averaged over all particles of a given atom type to compute the mean coordination number (--*CN*) {Note to typesetting: the two dash marks refer to a single overbar on top of *CN*; in italics to represent the variable: mean coordination number; please apply throughout, including figure captions}. The

radial length used for counting neighboring atoms was the distance to the minimum following the first peak in the radial distribution function for the corresponding atom pair.

Thermodynamics

MD simulation results

The MD simulation results cover -0.41 to 42 GPa and 3041 to 5172 K (EA-1). Figure 1 portrays the full range of P-T-ρ used to develop the EOS. Our fit included all state points in order to confidently describe liquid $NaAlSi_3O_8$ within the ranges 0–30 GPa and 3067–5132 K.

Tables in EA-2 contain thermodynamic properties computed from the EOS, arranged in regular P and T intervals. These tables can be used to interpolate thermodynamic properties of molten $NaAlSi_3O_8$ within the P-T-ρ of this study. Here we present a brief synopsis illustrating the effects of P and T on several thermodynamic properties. Discussions of sonic speed and the Grüneisen parameter are included in Appendix 1.

Internal energy. The calculated E values from all simulations were used in the EOS development, and EOS-predicted values are shown in Figure 2a. E monotonically increases with T, with typical values of -11.9×10^3 to -11.0×10^3 kJ/mol from 3000 to 5000 K at 5 GPa. At low P, E isothermally decreases upon compression. Shallow energy minima are noted for every isotherm, with minima occurring at higher P with increasing T. After the minima, E increases with P slower than the decrease at low P (Figure 2a). From standard thermodynamic identities, it is noted that $(\partial E/\partial P)_T = V(\beta_T P - \alpha T)$, and hence, the minima depicted in Figure 2a correspond to the P-T conditions where $\alpha T = \beta_T P$.

Heat capacity. The isochoric heat capacity ($C_V \equiv (\partial E/\partial T)_V$) is a straightforward derivative from the thermodynamic EOS. Tabulated values of C_V are given in EA-2. Figure 2b shows C_V as a function of P. For all T, C_V monotonically decreases with P, and all isotherms

approach an asymptote at high P (Figure 2b). C_V also decreases with increasing T. Over the P range of interest at 4000 K, C_V changes from about 440 J mol^{-1} K^{-1} to 380 J mol^{-1} K^{-1}.

Thermal pressure coefficient. The thermal pressure coefficient ($P_{th} \equiv (\partial P/\partial T)_V$) is the slope of each isochore in Figure 1. Values derived from the EOS fit are reported in EA-2 and five isotherms are shown in Figure 3a. P_{th} increases monotonically with P from 0 to 30 GPa but weakly depends on T at P < ~12 GPa (Figure 3a). A prominent T-dependence is apparent above ~12 GPa, with low-T isotherms showing the highest P_{th}. All isotherms converge near 11 GPa on a value of ~0.003 GPa/K. The locations of E minima in Figure 2a correspond to the conditions where P_{th} is identically equal to P/T.

Isobaric expansivity and isothermal compressibility. Isothermal compressibility (β_T) was calculated directly from the EOS. Expansivity (α) can be computed using β_T and the definition $P_{th} = \alpha/\beta_T$. Values for α and β_T are listed in EA-2 and displayed with P in Figures 3b and 3c, respectively.

Below 10 GPa, α decreases sharply with P but thereafter asymptotically approaches a fixed value. The exception occurs along low-T isotherms, where α shows a minimum value with P (e.g., 3000 K isotherm in Figure 3b). For T > 3500 K, however, α has no minima and monotonically decreases. At P < ~15 GPa, α increases with T, but the pattern reverses at higher P. At 4000 K from 0 to 12 GPa, α drops from ~1.3×10^{-4} to 4.0×10^{-5} K^{-1}, respectively. A typical value for α near 30 GPa is 3.4×10^{-5} K^{-1}.

Isothermal compressibility for liquid $NaAlSi_3O_8$ decreases monotonically with P over all T (Figure 3c). Along an isotherm, β_T rapidly decreases in the range 0–10 GPa but then follows a gentler slope at higher P. T has little effect on β_T except for P < 5 GPa where β_T increases with T

(Figure 3c). A typical value at low P is 0.08 GPa^{-1} at 4000 K. At high P, and for all isotherms, β_T approaches 0.006 GPa^{-1} (Figure 3c).

Comparison with laboratory thermodynamic data

The V-T relationship for liquid $NaAlSi_3O_8$ at 1 bar is well documented from laboratory experiments (Stein et al. 1986; Lange 1996; Anovitz and Blencoe 1999; Tenner et al. 2007). Near 1850 K and 1 bar, the value of α extrapolated from the present study is 4.1×10^{-5} K^{-1}, which falls between values extrapolated from Stein et al. (1986) and Lange (1996). At 2500 K—still above the experimental T—our work extrapolates to $\alpha = 7.98 \times 10^{-5}$ K^{-1}, which is 1.88 and 2.45 times larger than those extrapolated from Stein et al. (1986) and Lange (1996), respectively.

The isothermal compressibility from this work shows similar trends as those from the piston-cylinder experiments of Tenner et al. (2007). Their values for β_T at 1773 K decrease with P and follow the same trend shown in Figure 3c. Around 2035 K, values extrapolated from our study agree with the work of Kress et al. (1988) and give $\beta_T \cong 5.85 \times 10^{-2}$ GPa^{-1}. Below 2035 K, our work predicts lower β_T than those from experiment (Kress et al. 1988).

Isobaric heat capacity (C_P) for liquid $NaAlSi_3O_8$ has been measured by drop calorimetry at 1 bar in the range 900–1800 K (Richet and Bottinga 1980, 1984; Stebbins et al. 1982, 1983). Richet and Bottinga (1984) report a T-dependent C_P, which ranges from ~347 to 386 J mol^{-1} K^{-1} between 1096 and 2000 K. Stebbins et al. (1983) provide a T-independent C_P of ~369 J mol^{-1} K^{-1} up to 1810 K at 1 bar. Tenner et al. (2007) combined data from Stebbins et al. (1983) and Richet and Bottinga (1984) to calculate a T-independent C_P value of 359 ± 4 J mol^{-1} K^{-1} from 1182 to 1810 K at 1 bar.

We calculated C_P for liquid $NaAlSi_3O_8$ from the relationship

— (6)

using the properties derived from the EOS (EA-2). For $T < 2500$ and 1 bar, the extrapolated C_P is near 500 J mol^{-1} K^{-1} and increases slightly with increasing T. These results from the EOS are 16–27% higher at 1 bar than the extrapolated C_P of Richet and Bottinga (1984) between 2100 and 3100 K. Compared to Stebbins et al. (1983), our value of C_P is about 34% higher at 1800 K. Since our α and β_T are, respectively, higher and lower than those measured in the laboratory, it is expected that C_P is larger than experimental values (see Equation 6). Additionally, the extrapolated comparisons were at 1 bar, but the MD uncertainty in P is about 2 kbar. C_V has a strong P-dependence at low P (Figure 2b), and consequently, the uncertainty in P could reasonably explain the 1-bar mismatch in C_P (Equation 6). Appreciating the large extrapolation in T (between ~1800 and 3100 K) also softens the C_P discrepancy and demonstrates that, within error, the EOS reproduces experimentally-measured thermodynamic properties of liquid $NaAlSi_3O_8$.

Internal pressure results and discussion

P_{int}^F was determined from the EOS using the right hand side of Equation 3 (EA-2). Figure 4a depicts the variation of P_{int}^F with P along several isotherms from 3000 to 5000 K. For P in the range 0–17 GPa (depending on T), P_{int}^F is negative—indicating that attractive forces dominate over repulsion. The transition from attractive to repulsive dominance occurs at higher P as T increases. Above ~17 GPa, repulsive forces dominate at all T of this study.

Figure 4b shows P_{int}^F plotted versus T. Attractive forces dominate at $P < 5$ GPa for all T. For P in the range 1 bar to 2 GPa, the internal pressure is roughly T independent. As expected, conditions of low P and high T favor attractive forces, and the opposite trend is observed at high P and low T (Figure 4).

Internal pressure is dominated by inter-atomic attraction at high T and low P because the large kinetic energy of the system causes the forces to "hold tightly" to the moving atoms while the low P does not "tightly" constrain the particles. Conversely, in the low-T and high-P regimes, the particles are being "squeezed" together; thus, there are stronger repulsive forces acting between atoms. As discussed below, regions of P and T where attractive forces dominate ($P_{int}^{F} < 0$) correlate with the most profound changes in melt structure. The change in inter-atomic forces (across $P_{int}^{F} = 0$) with P matches several patterns in structural and transport properties, including the packing density of O (the most abundant atom), the stabilizing of structure, and trends in diffusion.

Self-diffusion

Self-diffusivity results

Self-diffusivities in liquid $NaAlSi_3O_8$ typically order $D_{Na} > D_{Al} > D_O > D_{Si}$ at a given state point (EA-1). All species show an isobaric increase in D with increasing T (Figure 5). In general, D decreases upon compression. At ~5132 K, D_{Na} decreases by a factor of ~6 from 0 to 30 GPa (Figure 5a). Over the same P-T conditions, the diffusivities for Al, Si, and O decrease by factors of about 2.7, 2.8, and 3.0, respectively. The relative decrease in D with compression is reduced at lower T (Figure 5). Along the 3067 ± 18 K pseudo-isotherm, Al, Si, and O have a concave-down trend, with maxima between 3.2 and 6.2 GPa (Figures 5b, 5c, and 5d).

Changes in D with P are most rapid at low P for all atom types, although this can be seen most readily for Na (Figure 5a). In the Arrhenius model, the magnitude of the rate of change of D_{Na} with P along an isotherm ($|\partial D_{Na}/\partial P|_T$) decreases upon compression and is approximately zero near 30 GPa (solid lines in Figure 5a). Model curves for D_{Al}, D_{Si}, and D_O also demonstrate

reduction in slope magnitude with compression (most notably along the highest isotherms) but lack the strong concavity of D_{Na}.

All D values from the MD simulations were fit to a modified Arrhenius expression to obtain activation energies and volumes. The modified Arrhenius expression has the form:

(7)

where E^* is the activation energy, D_0 is a pre-exponential constant, and the parameters v_0, v_1, and v_2 are linear coefficients for the activation volume ($V^* = v_0 + v_1P + v_2T$). Calculated constants for Equation 7 are listed by species in Table 2. E^* ranked Na < Al < O < Si over the T and P of this work with values of 85.0 and 140 kJ/mol for Na and Si, respectively. All fits to the Arrhenius expression have an R^2 greater than 0.976 (Table 2).

Self-diffusion discussion and laboratory comparison

Diffusivities of various alkali elements in $NaAlSi_3O_8$ glass were investigated at ambient pressure (Jambon and Carron 1976). For 623–1068 K, D_{Na} falls between 2.1×10^{-14} and 1.1×10^{-10} m^2/s (Jambon and Carron 1976). D_{Na} at 1 bar from our Arrhenius model yields 4.1×10^{-14} and 3.8×10^{-11} m^2/s at 623 and 1068 K, respectively—within a factor of three of experiments.

Baker (1995) used Ga as a tracer analogue for Al diffusion in liquid $NaAlSi_3O_8$, reporting an estimate of D_{Si} between 7.5×10^{-17} and 3.4×10^{-14} m^2/s at 1438 and 1831 K, respectively. Diffusivity of Ga (D_{Ga})—as a proxy for D_{Al}—was 7.6×10^{-17} and 1.8×10^{-13} m^2/s at 1427 and 1775 K, respectively (Baker 1995). By extrapolating to low T, our results are faster by several orders of magnitude but show the same relationship: $D_{Al} > D_{Si}$.

Poe et al. (1997) reported D values for various sodium-silicate liquids. For $NaAlSi_3O_8$ at 2100 K, D_O spans from about 1.8×10^{-11} to 4×10^{-11} m^2/s over the range 2–6 GPa (Poe et al. 1997). These are comparable to our extrapolation of ~3×10^{-10} m^2/s down to 2100 K at 6 GPa.

Diffusivities in liquid $NaAlSi_3O_8$ generally decrease with increasing *P*, but at ~3067 K, Al, Si, and O show an increase in diffusivity with *P* up to ~5 GPa. Several experiments have reported this anomalous *P* effect for diffusion in sodium-silicate liquids (including $NaAlSi_3O_8$) between ~1700 and 2800 K (Shimizu and Kushiro 1984; Rubie et al. 1993; Poe et al. 1997; Tinker et al. 2003). The work of Poe et al. (1997) on $NaAlSi_3O_8$ liquid revealed a maximum in D_O near 5 GPa at 2100 K, which is very similar to the low-*T* results of the MD simulations (Figure 5d). At $T > 3067$ K, however, the anomalous *P* effect seems to dissipate—as suggested by the reverse concavity in the pseudo-isotherms for D_{Al}, D_{Si}, and D_O at low *P* (Figures 5b, 5c, and 5d). We infer, therefore, that the anomalous *P* effect on self-diffusivity in liquid $NaAlSi_3O_8$ is present at high *T* but disappears above ~3100–3300 K.

Activation energies (E^*, listed in Table 2) for liquid $NaAlSi_3O_8$ were calculated from diffusion results over the entire *P*-*T* regime of interest (EA-1). Our work spans a range of ~2000 K and 30 GPa—considerably larger than most experimental work—and we again stress the necessity to consider the *T* range upon which *D* models are based (see Theory and Calculations section). Na activation energy for self-diffusion in $NaAlSi_3O_8$ glass at 623–1068 K is 56.5 ± 12.6 kJ/mol (Jambon and Carron 1976). E^* for Na in the MD-simulated liquid is 50% larger than the value of Jambon and Carron (1976), but the large difference in *T* and in the *T* range make this an indirect comparison.

Diffusion coefficients for all atom types in liquid $NaAlSi_3O_8$ have a systematic pattern with respect to *E*. In Figure 6, the EOS model for *E* versus the Arrhenius fit for *D* is shown at several isotherms. *P* increases from right to left along an isotherm in these coordinates. Since *D* (in general) monotonically decreases with increasing *P*, the pattern in Figure 6 mirrors that of the *P*-dependence of *E* along an isotherm (Figure 2a). For a given *T*, *D* increases with *E* at low *P*

and decreases with increasing E at high P. Each isotherm has a similar concave-up shape among all atom types, but the diffusion curves for Al, Si, and O show greater similarity than those of D_{Na} (Figure 6). The D_{Na} curves have a broader base than D_{Al}, D_{Si}, and D_O (Figure 6). These characteristics distinguish the network modifier (Na) cations from the network formers (Al and Si) and from the anionic "matrix" (O). Absolute values of and thermodynamic trends in D_{Al}, D_{Si}, and D_O are very similar, suggesting cooperative mobility among Al, Si, and O in aluminosilicate melt at high T and P.

Structure

Coordination statistics from MD results

The mean coordination number of O around a central Si atom (--CN_{SiO}) increases from ~4 to 4.9 between 0 and 30 GPa (Figure 7a). A similar pattern is noted for --CN_{AlO} (O around Al), which changes more rapidly from ~4 to 5.5 in the same P interval (Figure 7b). Both --CN_{SiO} and --CN_{AlO} appear T-independent, having approximately constant values for all T at specified P. However, --CN_{SiO} increases with P in a generally linear fashion while --CN_{AlO} has a slight concave-down pattern.

Overall, --CN_{OO} increases from ~8–8.5 at 1 bar to ~12.5–13 at 30 GPa. Along each pseudo-isotherm, --CN_{OO} increases with P except for a slight drop occurring between ~7 and 20 GPa (Figure 7c). As T increases, this small drop in --CN_{OO} occurs at higher P. The only exception to this T pattern is near 4000 K: at 3945 ± 20 K, --CN_{OO} shows a drop at 15.5 GPa, and at 4242 ± 19 K, the drop occurs at 13.6 GPa (Figure 7c). Of greater interest is the overarching convex shape of --CN_{OO} with respect to P.

At 5132 ± 21 K, --CN_{NaO} ranges from ~5.0 to 9.1 between 0 and 30 GPa, and at 3067 ± 18 K, this varies from ~7.5 to 9.9 (Figure 7d). Three clusters of maxima peaks in --CN_{NaO} are

visible for all *T* near 3, 10, and 22 GPa (Figure 7d). Peaks at low *P* are extremely variable with *T*, and several pseudo-isotherms have multiple peaks. Rapid changes occur at low *P* along an isotherm, but after ~10 GPa, --CN_{NaO} is less variable with *P* (Figure 7d). In general, both --CN_{OO} and --CN_{NaO} decrease with increasing *T*, although irregular exceptions are found at low *P*.

Fractions of Si-O and Al-O polyhedra coordination with *P* are shown in Figures 8 and 9, respectively. There is a slight *T*-dependence on the fraction amounts, but the effect of *P* on the distribution is more pronounced. The abrupt kinks in polyhedra fractions at 4242 ± 19 K and ~15 GPa (Figures 8b and 9b) were analyzed in relation to (1) the fluctuation in *P* and *T* inherent to the microcanonical ensemble, (2) the variation in *T* along a pseudo-isotherm, (3) *E* values from the MD results, and (4) diffusion trends. As explained in Appendix 2, none of these sources of error or thermodynamic properties satisfactorily explain the kink features. It is possible that these kinks simply reflect the scatter in the MD results. Further research may help resolve this issue.

Most Si-O and Al-O polyhedra are 4-, 5-, or 6-fold coordinated. Four-fold structures decrease with *P* while 5-fold structures increase and maximize. Six-fold coordination increases continuously with *P*, becoming most abundant after the peak in 5-fold structures. The amount of 2-, 3-, and 7-fold structures increases with *T*—most notably for 3-fold polyhedra, which increase to 22% and 35% of Si-O and Al-O polyhedra, respectively, at ~5132 K and low *P*.

Maxima in the fraction of SiO_4 and AlO_4 polyhedra (tetrahedra) are evident near 1.5 GPa for 4242 ± 19 K and near 3 GPa for 5132 ± 21 K. Si-O and Al-O polyhedra are most abundantly in 4-fold coordination until ~20 GPa and 7 GPa, respectively. With further compression, the liquid structure becomes dominated by SiO_5 and AlO_5 polyhedra, which persist over a broad range in *P* (Figures 8 and 9). AlO_5 polyhedra fractions maximize between 15 and 20 GPa

(depending on T) with peak values of ~0.48 at 3059 K and ~0.44 at 5136 K. In contrast, the SiO_5 peaks occur above 30 GPa, with apparent fractions close to 0.50.

Interrelationship between structure, thermodynamics, and self-diffusion

The fractional distribution of Al-O and Si-O coordination is strongly dependent on P, consistent with trends discovered in experiment. Spectroscopic studies of $NaAlSi_3O_8$ glasses have reported increases in Al-O coordination with P for over 25 years (Stebbins and Sykes 1990; Li et al. 1995; Yarger et al. 1995; Lee et al. 2004; Allwardt et al. 2005; Gaudio et al. 2015). Analyzing quenched glasses of $NaAlSi_3O_8$-$Na_2Si_4O_9$ composition, Yarger et al. (1995) reported increasing amounts of AlO_5 and AlO_6 polyhedra with P up to 12 GPa. Recent NMR work on annealed $NaAlSi_3O_8$ glass around 1000 K showed --CN_{AlO} increasing from 4.0 to 4.74 between ~1 bar and 10 GPa (Allwardt et al. 2005; Gaudio et al. 2015). A similar increase in --CN_{AlO} is seen at the lowest T of the present study (Figure 7b). Peaks in the 5-fold coordination fractions of Al-O occur at nearly half the P of those for Si-O polyhedra (Figures 8 and 9). This relationship supports the observation that Al coordination begins to change at a lower P than Si for a variety of aluminosilicates (Waff 1975; Williams and Jeanloz 1988; Yarger et al. 1995).

Additionally, we used the fractional distributions of polyhedra to derive a simple thermodynamic speciation model (see Appendix 3).

The convex shape of --CN_{AlO}, --CN_{OO}, and --CN_{NaO} with P reflects the stabilizing effect of the forces measured by P_{int}^F. As shown in Figure 4a, the P at which $P_{int}^F = 0$ ranges from ~6 to ~17 GPa (depending on T), signifying the change from attractive to repulsive inter-atomic forces upon compression. At P between these bounds (6–17 GPa), --CN transitions from rapid increases (at low P) to gentler increases (at high P). We submit that the thermodynamic property P_{int}^F acts as a measure of stabilization of liquid structure in $NaAlSi_3O_8$.

At high P, O-O polyhedra approach the form of an icosahedron (CN = 12). This structure exhibits high packing efficiency relative to other coordination states (Kottwitz 1991; Spera et al. 2011). Maximizing the shortest distance between atoms is demonstrably the same as minimizing the repulsive energy between pair-wise particles (Leech 1957). We speculate that because Born (electron) repulsion dominates the inter-atomic field in liquid $NaAlSi_3O_8$ at high P, the minimization of repulsive energy drives the O-O polyhedra toward an icosahedron configuration. This phenomenon of icosahedral O packing was noted in liquid $MgSiO_3$ using the Matsui (1998) potential (Spera et al. 2011). Icosahedra of O may be a general feature of all silicate liquids at high P and could explain the observed slow rate of change of melt structure at high P.

Structural stabilization at higher P is also concordant with the general slowing of the rate of change of diffusion with P (i.e., the decrease in $|\partial D/\partial P|_T$). The most rapid changes in --CN occur at low P and correspond to the largest $|\partial D/\partial P|_T$, particularly at high T (Figure 10). With increasing P, the structure gradually stabilizes as $|\partial D/\partial P|_T$ decreases. These observations are consistent with a densely-packed structure at high P that restricts ion mobility.

Compressional changes in D and --CN are not identical between atom types. Network modifier atoms (Na) typically move through the structure with the highest D values at a given state point. O diffuses at similar rates as those of the network formers (Al and Si), perhaps with cooperative flow (cf. Bryce et al. 1999). Despite this similarity between O, Al, and Si, the --CN_{OO} changes more rapidly at low P than --CN_{AlO} or --CN_{SiO} (Figure 10). The latter two are especially similar (in both magnitude and rate of change), which can be readily understood considering the comparable roles of Al-O and Si-O polyhedra in a network silicate structure. --CN_{OO} appears to change with P in greater similarity to --CN_{NaO}, yet the diffusivity of O behaves more like D_{Al} and D_{Si} (Figure 10).

During isothermal compression, D_{Na} seems to approach the value of D_{Al} (and D_{Si} and D_O) at P > ~20 GPa. This is illustrated by the spread in MD-calculated D values (across all atom types) at a given state point. At low P, the spread in D values is ~68–90% of D_{Na} (depending on T), dropping to ~26–35% of D_{Na} at P > 20 GPa. Therefore, as inter-atomic repulsive forces lead to greater packing efficiency of ions at high P, the high-density structure may also give rise to greater similarity in D values among all species in liquid $NaAlSi_3O_8$.

Implications

A robust EOS for liquid $NaAlSi_3O_8$ is herein provided and gives a self-consistent view of the thermodynamics at elevated P and T. From the EOS, thermodynamic properties are calculated within the ranges 3067–5132 K and 0–30 GPa, and extrapolations outside these regimes provide reasonable estimates. We have shown that the fundamental-measure functional of Rosenfeld and Tarazona (1998) reliably models liquid $NaAlSi_3O_8$ at high T and P, demonstrating the applicability of the $T^{3/5}$ scaling relationship to sodium-aluminosilicate liquids.

Results suggest an "anomalous diffusion" region for Al, Si, and O at P < 10 GPa and 3067 ± 19 K (the lowest T of this study). At higher T, the anomaly is absent for these species, indicating that the upper T limit for anomalous diffusion in liquid $NaAlSi_3O_8$ falls in the range 3067–3353 K. Formation of high-coordinated Al-O structures initiates a lower P than those of Si-O—in support of the long-standing discussion about structural changes in aluminosilicate liquids (Waff 1975). The explanation for high-P coordination of O-O polyhedra based on packing theory and inter-atomic potential energy may be applicable to all silicate liquids.

Internal pressure is a measure of inter-atomic forces between structural components in fluids (Kartsev et al. 2012). With isothermal compression, the dominant forces in liquid $NaAlSi_3O_8$ change from attraction to repulsion. At P < ~6 GPa, the liquid structure changes

rapidly with increasing P as shown in the --CN and coordination fractions of the polyhedra. These rapid structural changes begin to slow and stabilize concurrently with the transition in the inter-atomic forces (near $P_{int}^{F} = 0$) and with the decrease in $|\partial D/\partial P|_T$. Several thermodynamic properties (e.g., E, α, β_T) also change less rapidly at higher P, suggesting that the stabilizing effect on liquid structure by inter-atomic repulsive forces correspondingly acts on the high-P self-diffusion and thermodynamics of liquid $NaAlSi_3O_8$.

Acknowledgements

The authors express appreciation to two anonymous reviewers for detailed and extensive commentary on the manuscript. This research used resources of the National Energy Research Scientific Computing Center (NERSC), a DOE Office of Science User Facility. NERSC is supported by the Office of Science of the U.S. Department of Energy under Contract Number DE-AC02-05CH11231.

References

Allen, M.P., and Tildesley, D.J. (1987) Computer Simulation of Liquids, 385 p. Oxford University Press, New York.

Allwardt, J.R., Poe, B.T., and Stebbins, J.F. (2005) Letter. The effect of fictive temperature on Al coordination in high-pressure (10 GPa) sodium aluminosilicate glasses. American Mineralogist, 90, 1453-1457.

Angell, C.A., Cheeseman, P.A., and Tamaddon, S. (1982) Pressure enhancement of ion mobilities in liquid silicates from computer simulation studies to 800 kilobars. Science, 218, 885-887.

Anovitz, L.M. and Blencoe, J.G. (1999) Dry melting of high albite. American Mineralogist, 84, 1830-1842.

Arndt, J., and Häberle, F. (1973) Thermal expansion and glass transition temperatures of synthetic glasses of plagioclase-like compositions. Contributions to Mineralogy and Petrology, 29, 175-183.

Baker, D.R. (1995) Diffusion of silicon and gallium (as an analogue for aluminum) network-forming cations and their relationship to viscosity in albite melt. Geochimica et Cosmochimica Acta, 59, 3561-3571.

Bryce, G.J., Spera, F.J., and Stein, D.J. (1999) Pressure dependence of self-diffusion in the $NaAlO_2$-SiO_2 system: Compositional effects and mechanisms. American Mineralogist, 84, 345-356.

Coluzzi, B., and Verrocchio, P. (2002) The liquid-glass transition of silica. The Journal of Chemical Physics, 116, 3789-3794.

Creamer, J.B. (2012) Modeling fluid-rock interaction, melt-rock interaction, and silicate melt properties at crustal to planetary interior conditions, 104 p. Ph.D. thesis, University of California, Santa Barbara.

Cygan, R.T. (2001) Molecular modeling in mineralogy and geochemistry. In R.T. Cygan and J.D. Kubicki, Eds., Molecular Modeling Theory: Applications in the Geosciences, 42, p. 1-35. Reviews in Mineralogy and Geochemistry, Mineralogical Society of America, Chantilly, Virginia.

Gaudio, S.J., Lesher, C.E., Maekawa, H., and Sen, S. (2015) Linking high-pressure structure and density of albite liquid near the glass transition. Geochimica et Cosmochimica Acta, 157, 28-38.

Ghiorso, M.S. (2004a) An equation of state for silicate melts. I. Formulation of a general model. American Journal of Science, 304, 637-678.

Ghiorso, M.S. (2004b) An equation of state for silicate melts. III. Analysis of stoichiometric liquids at elevated pressure: Shock compression data, molecular dynamics simulations and mineral fusion curves. American Journal of Science, 304, 752-810.

Ghiorso, M.S., Nevins, D., Cutler, I., and Spera, F.J. (2009) Molecular dynamics studies of $CaAl_2Si_2O_8$ liquid. Part II: Equation of state and a thermodynamic model. Geochimica et Cosmochimica Acta, 73, 6937-6951.

Hockney, R.W., and Eastwood, J.W. (1988) Computer Simulation Using Particles, 540 p. IOP Publishing Ltd., Bristol, Great Britain.

Ingebrigtsen, T.S., Veldhorst, A.A., Schrøder, T.B., and Dyre, J.C. (2013) Communication: The Rosenfeld-Tarazona expression for liquids' specific heat: A numerical investigation of eighteen systems. The Journal of Chemical Physics, 139, 171101/1-4.

Jambon, A., and Carron, J.P. (1976) Diffusion of Na, K, Rb and Cs in glasses of albite and orthoclase composition. Geochimica et Cosmochimica Acta, 40, 897-903.

Kartsev, V.N. (2004) To the understanding of the structural sensitivity of the temperature coefficient of internal pressure. Journal of Structural Chemistry, 45, 832-837.

Kartsev, V.N., Shtykov, S.N., Pankin, K.E., and Batov, D.V. (2012) Intermolecular forces and the internal pressure of liquids. Journal of Structural Chemistry, 53, 1087-1093.

Kottwitz, D.A., (1991) The densest packing of equal circles on a sphere. Acta Crystallographica Section A, 47, 158-165.

Kress, V.C., Williams, Q., and Carmichael, I.S.E. (1988) Ultrasonic investigation of melts in the system Na_2O-Al_2O_3-SiO_2. Geochimica et Cosmochimica Acta, 52, 283-293.

Kushiro, I. (1978) Viscosity and structural changes of albite ($NaAlSi_3O_8$) melt at high pressures, Earth and Planetary Science Letters, 41, 87-90.

Lacks, D.J., Rear, D.B., and Van Orman, J.A. (2007) Molecular dynamics investigation of viscosity, chemical diffusivities and partial molar volumes of liquids along the MgO–SiO_2 join as functions of pressure. Geochimica et Cosmochimica Acta 71, 1312-1323.

Lange, R.A. (1996) Temperature independent thermal expansivities of sodium aluminosilicate melts between 713 and 1835 K. Geochimica et Cosmochimica Acta, 60, 4989-4996.

Lay, T., Hernlund, J., and Buffett, B.A. (2008) Core-mantle boundary heat flow. Nature Geoscience, 1, 25-32.

Lee, S.K., Cody, G.D., Fei, Y., and Mysen, B.O. (2004) Nature of polymerization and properties of silicate melts and glasses at high pressure. Geochimica et Cosmochimica Acta, 68, 4189-4200.

Leech, J. (1957) Equilibrium of sets of particles on a sphere. The Mathematical Gazette, 41, 81-90.

Li, D., Secco, R.A., Bancroft, G.M., and Fleet, M.E. (1995) Pressure induced coordination change of Al in silicate melts from Al K edge XANES of high pressure $NaAlSi_2O_6$ - $NaAlSi_3O_8$ glasses. Geophysical Research Letters, 22, 3111-3114.

Martin, G.B., Spera, F.J., Ghiorso, M.S., and Nevins, D. (2009) Structure, thermodynamic, and transport properties of molten Mg_2SiO_4: Molecular dynamics simulations and model EOS. American Mineralogist, 94, 693-703.

Martin, G.B., Ghiorso, M., and Spera, F.J. (2012) Transport properties and equation of state of 1-bar eutectic melt in the system $CaAl_2Si_2O_8$-$CaMgSi_2O_6$ by molecular dynamics simulation. American Mineralogist, 97, 1155-1164.

Matsui, M. (1998) Computational modeling of crystals and liquids in the system Na_2O-CaO-MgO-Al_2O_3-SiO_2. In M.H. Manghnani and T. Yagi, Eds., Properties of Earth and Planetary Materials at High Pressure and Temperature, p. 145-151. Geophysical Monograph Series, American Geophysical Union, Washington, D.C.

Nevins, D.I.R. (2009) Understanding silicate geoliquids at high temperatures and pressures through molecular dynamics simulations, 221 p. Ph.D. thesis, University of California, Santa Barbara.

Nevins, D., and Spera, F.J. (2007) Accurate computation of shear viscosity from equilibrium molecular dynamics simulations. Molecular Simulation, 33, 1261-1266.

Oganov, A.R., Brodholt, J.P., and Price, G.D. (2000) Comparative study of quasiharmonic lattice dynamics, molecular dynamics and Debye model applied to $MgSiO_3$ perovskite. Physics of the Earth and Planetary Interiors, 122, 277-288.

Plimpton, S. (1995) Fast parallel algorithms for short-range molecular dynamics. Journal of Computational Physics, 117, 1-19. [lammps.sandia.gov]

Poe, B.T., McMillan, P.F., Rubie, D.C., Chakraborty, S., Yarger, J., and Diefenbacher, J. (1997) Silicon and Oxygen Self-Diffusivities in Silicate Liquids Measured to 15 Gigapascals and 2800 Kelvin. Science, 276, 1245-1248.

Rapaport, D.C. (1995) The Art of Molecular Dynamics Simulation, 400 p. Cambridge University Press, U.K.

Refson, K. (2001) Moldy User's Manual (rev. 2.25.2.6), 78 p. Department of Earth Sciences, University of Oxford.

Richet, P., and Bottinga, Y. (1980) Heat capacity of liquid silicates: new measurements on $NaAlSi_3O_8$ and $K_2Si_4O_9$. Geochimica et Cosmochimica Acta, 44, 1535-1541.

Richet, P., and Bottinga, Y. (1984) Glass transitions and thermodynamic properties of amorphous SiO_2, $NaA1Si_nO_{2n+2}$ and $KAlSi_3O_8$. Geochimica et Cosmochimica Acta, 48, 453-470.

Richet, P., and Bottinga, Y. (1986) Thermochemical properties of silicate glasses and liquids: A review. Reviews of Geophysics, 24, 1-25.

Rosenfeld, Y., and Tarazona, P. (1998) Density functional theory and the asymptotic high density expansion of the free energy of classical solids and fluids. Molecular Physics, 95, 141-150.

Rubie, D.C., Ross, C.R., II, Carroll, M.R., and Elphick, S.C. (1993) Oxygen self-diffusion in $Na_2Si_4O_9$ liquid up to 10 GPa and estimation of high-pressure melt viscosities. American Mineralogist, 78, 574-582.

Saika-Voivod, I., Sciortino F., and Poole, P.H. (2000) Computer simulations of liquid silica: equation of state and liquid-liquid phase transition. Physical Review E, 63, 011202/1-9.

Sastry, S. (2000) Liquid limits: Glass transition and liquid-gas spinodal boundaries of metastable liquids. Physical Review Letters, 85, 590-593.

Shimizu, N., and Kushiro, I. (1984) Diffusivity of oxygen in jadeite and diopside melts at high pressures. Geochimica et Cosmochimica Acta, 48, 1295-1303.

Spera, F.J., Nevins, D., Ghiorso, M., and Cutler, I. (2009) Structure, thermodynamic and transport properties of $CaAl_2Si_2O_8$ liquid. Part I: Molecular dynamics simulations. Geochimica et Cosmochimica Acta, 73, 6918-6936.

Spera, F.J., Ghiorso, M.S., and Nevins, D. (2011) Structure, thermodynamic and transport properties of liquid $MgSiO_3$: Comparison of molecular models and laboratory results. Geochimica et Cosmochimica Acta, 75, 1272-1296.

Stacey, F.D. (1995) Thermal and elastic properties of the lower mantle and core. Physics of the Earth and Planetary Interiors, 89, 219-245.

Stebbins, J.F. and Sykes, D. (1990) The structure of $NaAlSi_3O_8$ liquid at high pressure: New constraints from NMR spectroscopy. American Mineralogist, 75, 943-946.

Stebbins, J.F., Weill, D.F., Carmichael, I.S.E., and Moret, L.K. (1982) High temperature heat contents and heat capacities of liquids and glasses in the system $NaAlSi_3O_8$-$CaAl_2Si_2O_8$. Contributions to Mineralogy and Petrology, 80, 276-284.

Stebbins, J.F., Carmichael, I.S.E., and Weill, D.E. (1983) The high temperature liquid and glass heat contents and the heats of fusion of diopside, albite, sanidine and nepheline. American Mineralogist, 68, 717-730.

Stein, D.J., and Spera, F.J. (1995) Molecular dynamics simulations of liquids and glasses in the system $NaAlSiO_4$-SiO_2: Methodology and melt structures. American Mineralogist, 80, 417-431.

Stein, D.J., and Spera, F.J. (1996) Molecular dynamics simulations of liquids and glasses in the system $NaAlSiO_4$-SiO_2: Physical properties and transport mechanisms. American Mineralogist, 81, 284-302.

Stein, D.J., Stebbins, J.F., and Carmichael, I.S. (1986) Density of molten sodium aluminosilicates. Journal of the American Ceramic Society, 69, 396-399.

Tenner, T.J., Lange, R.A., and Downs, R.T. (2007) The albite fusion curve re-examined: New experiments and the high-pressure density and compressibility of high albite and $NaAlSi_3O_8$ liquid. American Mineralogist, 92, 1573-1585.

Tinker, D., Lesher, C.E., and Hutcheon, I.D. (2003) Self-diffusion of Si and O in diopside-anorthite melt at high pressures. Geochimica et Cosmochimica Acta, 67, 133-142.

Vinet, P., Ferrante, J., Smith, J.R., and Rose, J.H. (1986) A universal equation of state for solids. Journal of Physics C: Solid State Physics, 19, L467-L473.

Vinet, P., Smith, J.R., Ferrante, J., and Rose, J.H. (1987) Temperature effects on the universal equation of state of solids. Physical Review B, 35, 1945.

Vinet, P., Rose, J.H., Ferrante, J., and Smith, J.R. (1989) Universal features of the equation of state of solids. Journal of Physics: Condensed Matter, 1, 1941.

Waff, H.S. (1975) Pressure-induced coordination changes in magmatic liquids. Geophysical Research Letters, 2, 193-196.

Williams, Q., and Jeanloz, R. (1988) Spectroscopic evidence for pressure-induced coordination changes in silicate glasses and melts. Science, 239, 902-905.

Woodcock, L.V., Angell, C.A., and Cheeseman, P. (1976) Molecular dynamics studies of the vitreous state: Simple ionic systems and silica. The Journal of Chemical Physics, 65, 1565-1577.

Yarger, J.L., Smith, K.H., Nieman, R.A., Diefenbacher, J., Wolf, G.H., Poe, B.T., and McMillan, P.F. (1995) Al coordination changes in high-pressure aluminosilicate liquids. Science, 270, 1964-1967.

List of figure captions

Figure 1. MD simulation results for liquid $NaAlSi_3O_8$ shown as boxes in *P*-*T* space. Each box is centered on the average *P* and *T* values obtained from the respective MD simulation. The box size represents the one-sigma fluctuation in the *P* and *T* dimensions. Each line connecting the boxes is an isochore, with several density values listed adjacent to the respective line. Isochoric line spacing is 0.1 g/cm^3. The isochores for $\rho < 2.3$ g/cm^3 are not drawn for clarity.

Figure 2. (**a**) Internal energy, calculated from the EOS of this work, is shown as a function of *P* along several isotherms. (**b**) The isochoric heat capacity versus *P* is shown at different *T*.

Figure 3. Properties calculated from the EOS along various isotherms. (**a**) The thermal pressure coefficient $(\partial P/\partial T)_V$ is shown with *P*. (**b**) The isobaric expansion coefficient (expansivity) versus *P*. (**c**) The isothermal compressibility versus *P*.

Figure 4. Internal pressure expressed in terms of interatomic forces (P_{int}^F) versus (**a**) *P* and (**b**) *T*. When $P_{int}^F > 0$, the inter-atomic field is dominated by repulsive forces; $P_{int}^F < 0$ when internal forces are dominated by attraction (see text for discussion).

Figure 5. The *P*-dependence of self-diffusion coefficients is shown for (**a**) Na, (**b**) Al, (**c**) Si, and (**d**) O in liquid $NaAlSi_3O_8$. For all panels: symbols represent values calculated from the MD simulations along pseudo-isotherms, and solid lines represent isothermal curves generated from a modified Arrhenius model (Equation 7) using the values in Table 2. Not all pseudo-isotherms from the MD are drawn for clarity.

Figure 6. Internal energy (*E*, derived from the EOS) versus the self-diffusion of (**a**) Na, (**b**) Al, (**c**) O, and (**d**) Si. Diffusion values are calculated from the modified Arrhenius model (Equation 7) for the *T* shown and *P* between 0 and 30 GPa. *P* increases from right to left along an

isothermal curve. All panels have the same vertical (*E*) scale. Panels (**b**), (**c**), and (**d**) have the same horizontal (*D*) scale.

Figure 7. Average coordination numbers are shown with *P* at various *T* for (**a**) Si-O (i.e., O around Si), (**b**) Al-O, (**c**) O-O, and (**d**) Na-O polyhedra. Solid lines are principally for guiding the eye along an isotherm, connecting every MD result point with straight lines.

Figure 8. The distribution of Si-O polyhedra coordination at (**a**) 3067 ± 18 K, (**b**) 4242 ± 19 K, and (**c**) 5132 ± 21 K.

Figure 9. The distribution of Al-O polyhedra coordination at (**a**) 3067 ± 18 K, (**b**) 4242 ± 19 K, and (**c**) 5132 ± 21 K.

Figure 10. Composite plots of self-diffusion (marker symbols) and average CN (solid lines) versus *P*, from the MD simulations. (**a**) D_{Na} and --CN_{NaO} (average CN for O around Na), (**b**) D_{Al} and --CN_{AlO}, (**c**) D_{O} and --CN_{OO}, (**d**) D_{Si} and --CN_{SiO}. Diffusion symbols represent four pseudo-isotherms: 3067 ± 18 K (square), 3945 ± 20 K (diamond), 4534 ± 17 K (open circle), and 5132 ± 21 K (triangle). The same four pseudo-isotherms are shown for --*CN*, with thicker line width representing higher *T*. The average CN axis for (**c**) is drawn with same vertical exaggeration as the CN axis in (**a**). Note the linear scale for self-diffusion.

List of figure captions for figures in Appendices:

Figure A1. (**a**) Sonic speed versus *P*; calculated from the EOS analysis. (**b**) The Grüneisen parameter versus *P*. Note the crossover point near 18.4 GPa (see Appendix 1 text).

Figure A2. *T* variations along the 4242 ± 19 K pseudo-isotherm from the MD simulations, overprinted onto the Si-O polyhedra coordination fractions (compare to Figure 8b in the text).

Polyhedra fractions for SiO_3 and SiO_7 are not drawn for clarity. Horizontal dotted line indicates the average *T* (4242 K) from the 19 simulations with target *T* of 4200 K.

Appendices (text)

Appendix 1

Sonic speed

The bulk sonic speed (c) through a liquid is calculated from Equation A1:

$$\text{[illegible]} \qquad \text{(A1)}$$

where K is the isothermal bulk modulus ($\equiv 1/\beta_T$) (Ghiorso and Kress 2004). Figure A1a shows the speed of sound through liquid $NaAlSi_3O_8$ is largely P-dependent. Generally, c monotonically increases from about 2000 m/s at 1 bar to 7000 m/s near 30 GPa. The most rapid increase in c with P occurs at P < ~8 GPa. An apparent T-dependence in the c-P slope can be seen at high P, with higher T isotherms exhibiting steeper slopes (Figure A1a).

Grüneisen parameter

The Grüneisen parameter (γ), useful in relating thermoelastic properties at high P and high T, can be defined thermodynamically by Equation A2:

$$\text{[illegible]} \qquad \text{(A2)}$$

(Vočadlo et al. 2000). For liquid $NaAlSi_3O_8$, γ increases monotonically with P at all T of interest (Figure A1b). There is a stronger P-dependence on γ below 2 GPa than at higher P. A crossover point exists around 18.4 GPa, through which all isotherms pass at ~0.82 (Figure A1b). Below 18.4 GPa, γ increases with T at fixed P, and the pattern reverses at higher P.

References for appendix 1

Ghiorso, M.S., and Kress, V.C. (2004) An equation of state for silicate melts. III. Calibration of volumetric properties at 10^5 Pa. American Journal of Science, 304, 679-751.

Vočadlo, L., Poirer, J.P., and Price, G.D. (2000) Grüneisen parameters and isothermal equations of state. American Mineralogist, 85, 390-395.

Appendix 2

Kinks in polyhedra fractions at 4242 K

Figures 8b and 9b (for 4242 ± 19 K) of the main text show kinks near 15 GPa for the fraction curves of SiO_4, SiO_5, AlO_4, and AlO_6 (as well as in some of the minor polyhedra). We compared these fractions to the *T*-*P* relationship of the 4242 ± 19 K pseudo-isotherm (see Figure A2). Values of *P* along the target isotherm are known to within 0.29 GPa. The *T* (changing with *P* along the pseudo-isotherm) shows a minimum at 13.6 GPa, corresponding to the kinks in the SiO_4 and SiO_5 polyhedra fraction curves (Figure A2). For Al-O, the kinks in Figure 9b seem to be either concave at 13.6 or convex at 16.5 GPa, corresponding to a local *T* minimum (4222 K) or an "average" *T* (4247 K), respectively. It should be noted that the *T* minimum at 13.6 GPa is less extreme than the minima seen at 1.7 and 7.0 GPa (Figure A2). The *T* minimum at 1.7 GPa correlates with the polyhedra maxima of AlO_4 and SiO_4; this is a consistent relationship between *T* and the extrema in fractions of SiO_4 but is inconsistent with those of AlO_4. Additionally, the *T* minimum at 7.0 GPa is the most extreme, yet fractions in polyhedra show no kink patterns near this *P*. Although the *T* values from the simulations (for the 4200 K target isotherm) deviate from the averaged value (4242 K), the standard deviation in *T* does not explain the kinks in polyhedra fractions.

Another comparison was made with *E* from the simulation output (EA-1), which has a minimum (along the 4242 ± 19 K pseudo-isotherm) at 13.6 GPa. The *E* minimum at 13.6 GPa is very shallow, dropping ~0.1% between the adjacent values. This correlates with kinks in Si-O

polyhedra but is less convincing for Al-O fractions. From these observations, it is not clear that the *E* extrema is large enough to influence the polyhedra statistics.

Diffusivities were also analyzed with the coordination fractions. D_{Na} makes a very slight concave up shape at 13.6 GPa, which corresponds to the (convex) kink in SiO_4 fraction. This relationship may suggest that Na mobility decreases due to the increase in polymerization (where 4-fold coordination implies a tetrahedron structure and thus a more polymerized network) and decrease in the size of pathways through the structure. However, this relationship is not the same for AlO_4 abundances, and no other atom type exhibits a prominent feature in self-diffusion near 15 GPa. Thus, we conclude that diffusivity has little influence on the 15 GPa kinks in polyhedra fractions.

Appendix 3

Polyhedra equilibria

To further investigate the connection between thermodynamics and short-range liquid structure, we developed a thermodynamic equilibria model using the coordination statistics on Si-O, Al-O, and O-Si polyhedra. This simple model can be used to predict (to first-order approximation) the dependence of polyhedra abundances as a function of *P* and *T* over the *P*-*T* range of the MD simulations. Following the procedure in Morgan and Spera (2001), the method incorporates stepwise polyhedral equilibria and the law of mass action. For example, the concentrations of SiO_4, SiO_5, and SiO_6 are related via the equilibrium reaction

, (A3)

for which the change in Gibbs energy (ΔG) is zero at equilibrium. That is,

——— (A4)

where P° is a reference pressure, and H, S, and represent enthalpy, entropy, and the activity, respectively. We assume that the change in isobaric heat capacity (ΔC_P) is zero, the change in volume (ΔV) of the reaction is constant, and the polyhedra mix ideally. Based on these assumptions, Equation A4 reduces to

(A5)

with ΔH, ΔS, and ΔV remaining constant, and X representing number fractions from the coordination statistics of the corresponding polyhedra.

We used multiple linear regression models to extract values of ΔH, ΔS, and ΔV from Equation A5 for four polyhedra reactions. In addition to the SiO_5 polyhedra reaction (Equation A3), the following equilibria were analyzed:

(A6)

(A7)

. (A8)

Equations A6–A8 have the same form as that of Equation A3 and thus, under the same assumptions, follow the same development as Equation A5.

The thermodynamic parameters obtained from this analysis are collected in Table A1. All four polyhedra equilibrium regressions had an R^2 statistic above 0.88. Despite the approximations that (1) ΔH and ΔS for the reactions are independent of T, (2) ΔV of the reactions is constant and independent of P and T, and (3) mixing of polyhedra is ideal, the abundances of the various polyhedra are remarkably well recovered for a large span in P (~0–30 GPa) and T (~3100–5100 K) using the parameters of Table A1. This simple thermodynamic model shows promise for future MD studies of liquid structure as a means to quantify thermodynamic equilibria parameters.

References for appendix 3

Morgan, N.A., and Spera, F.J. (2001) A molecular dynamics study of the glass transition in $CaAl_2Si_2O_8$: Thermodynamics and tracer diffusion. American Mineralogist, 86, 915-926.

Tables

Table 1. The parameters for the potential of this work based on the effective pair-potential parameters of Matsui (1998).

Atom *i*	Atom *j*	A_{ij} (kcal/mol)	B_{ij} (Å)	C_{ij} (kcal-Å^6/mol)
Na	Na	3.142964E+11	8.00E-02	3.997392E+02
Na	Al	1.927601E+10	7.40E-02	3.597751E+02
Na	Si	5.777052E+11	6.30E-02	4.817195E+02
Na	O	3.346278E+06	1.78E-01	8.853671E+02
Al	Al	7.275557E+08	6.80E-02	3.238063E+02
Al	Si	1.686763E+10	5.70E-02	4.335593E+02
Al	O	6.562537E+05	1.72E-01	7.968521E+02
Si	Si	1.842153E+12	4.60E-02	5.805126E+02
Si	O	1.156812E+06	1.61E-01	1.066942E+03
O	O	1.489330E+05	2.76E-01	1.960966E+03

Table 2. The energy parameters from the Arrhenius fitting for self-diffusion in Equation (7).

Species	E^* (kJ/mol)	v_0 (cm^3/mol)	v_1 (cm^3 mol^{-1} GPa^{-1})	v_2 (cm^3 mol^{-1} K^{-1})	D_0 (m^2/s)	R^2
Na	85.028	2.152	-5.225E-02	3.596E-04	5.473E-07	0.9760
Al	118.982	-0.220	-1.040E-02	3.472E-04	5.664E-07	0.9881
Si	140.015	-0.884	-8.464E-03	4.606E-04	6.544E-07	0.9851
O	133.820	-0.753	-6.987E-03	4.650E-04	6.906E-07	0.9863

Note: E^* is the activation energy, D_0 is the pre-exponential, and the activation volume (V^*) is a linear function of P and T, i.e., $V^* = v_0 + v_1P + v_2T$.

Tables for appendices

Table A1. Thermodynamic parameters from the polyhedral equilibria (Equation A5).

Equilibrium reaction[a]	ΔS (J mol^{-1} K^{-1})	ΔV (m^3/mol)	ΔH (J/mol)	R^2
Eq. A3	12.95	-1.122E-07	7262.70	0.9669
Eq. A6	6.27	-2.484E-07	-12602.73	0.9089
Eq. A7	15.44	4.273E-07	-3402.29	0.9753
Eq. A8	5.96	1.380E-06	-82905.91	0.8860

[a] Equation number referenced in Appendix 3.

Figures

Figure 1

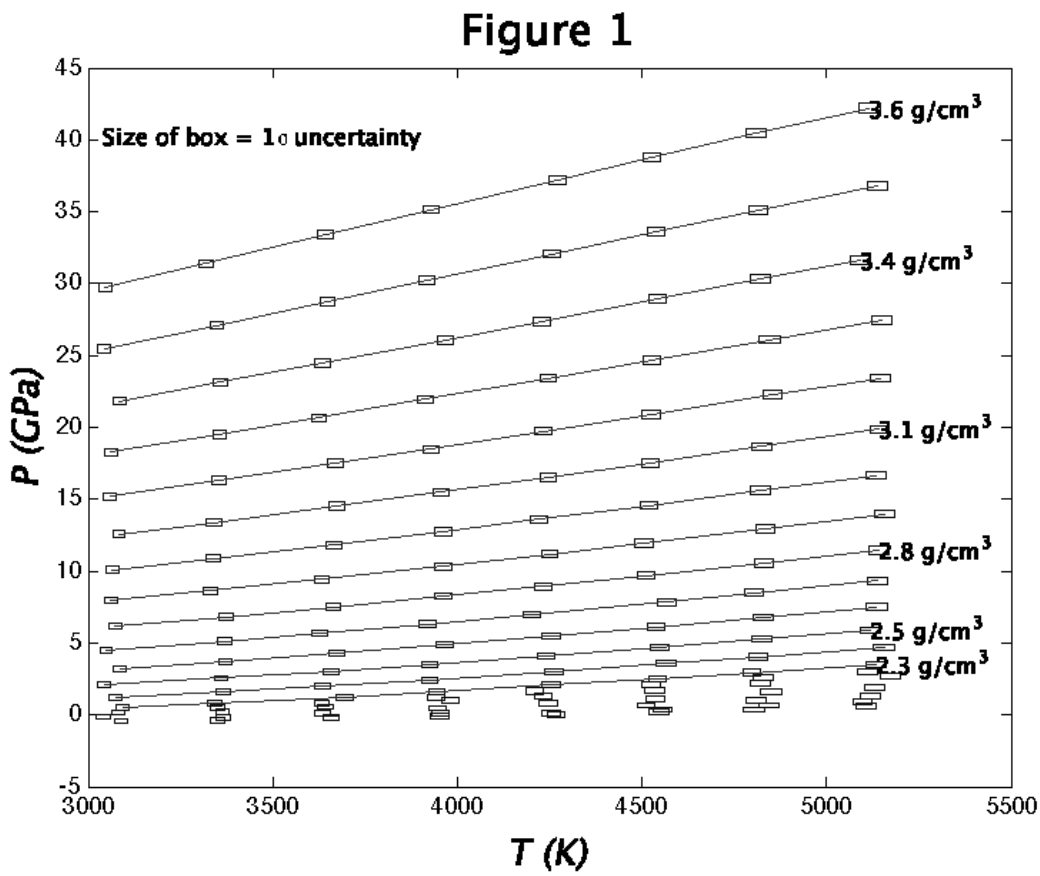

Figure 2

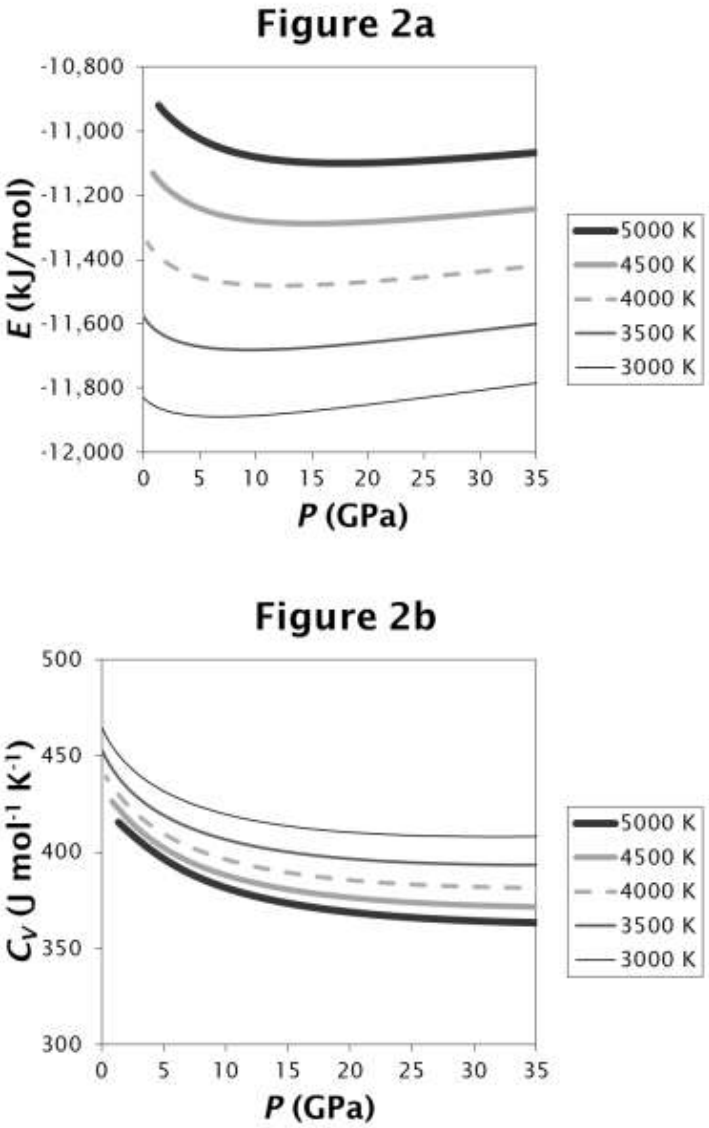

Figure 3

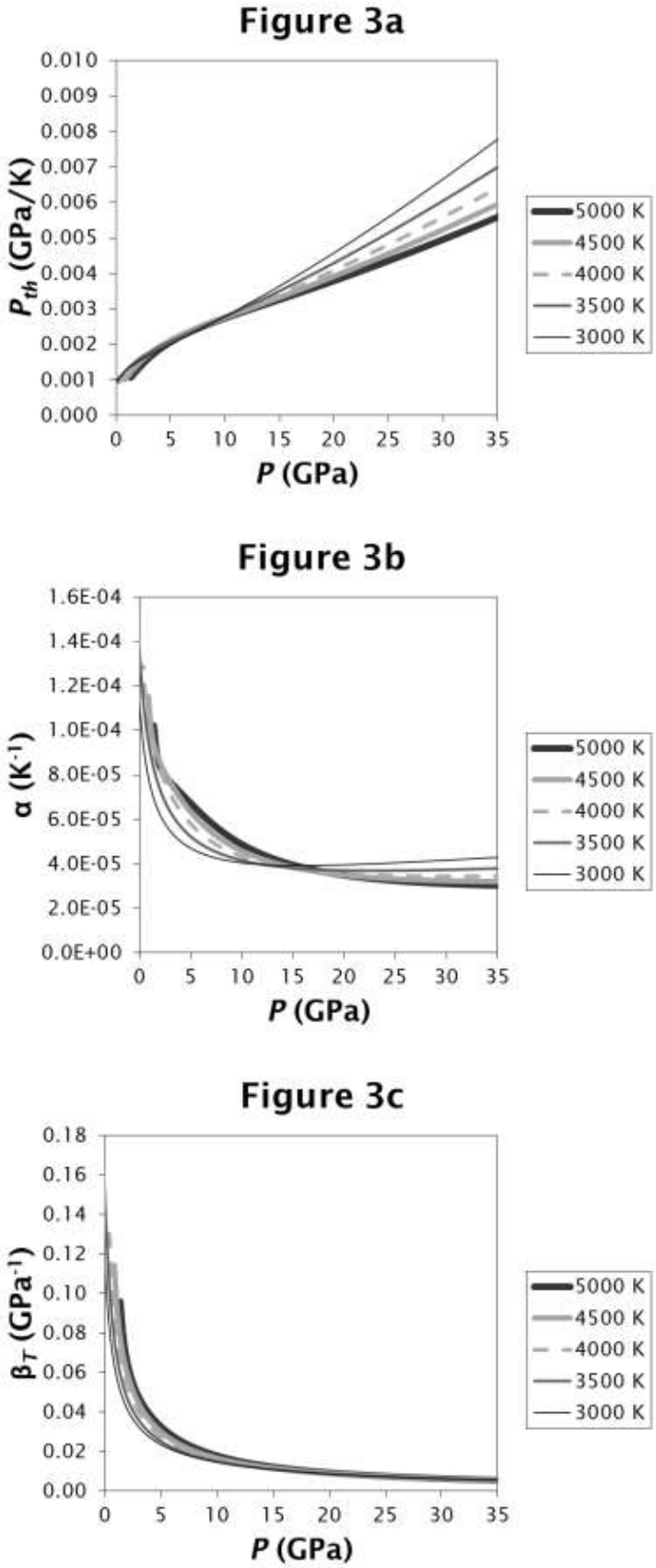

Figure 4

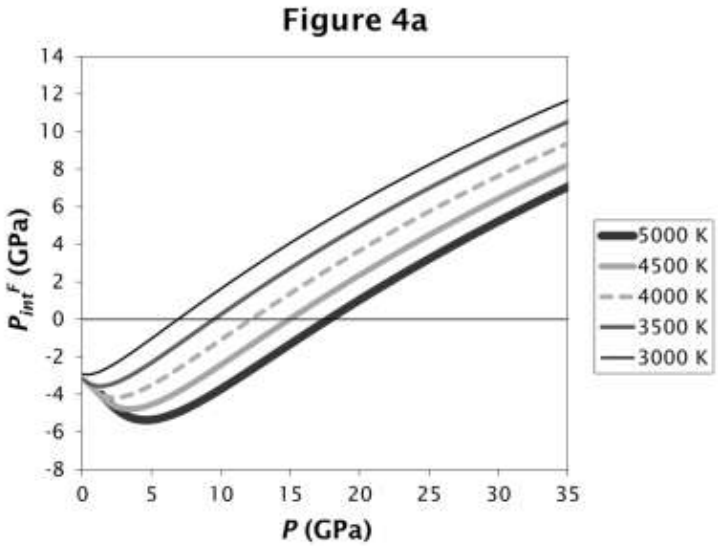

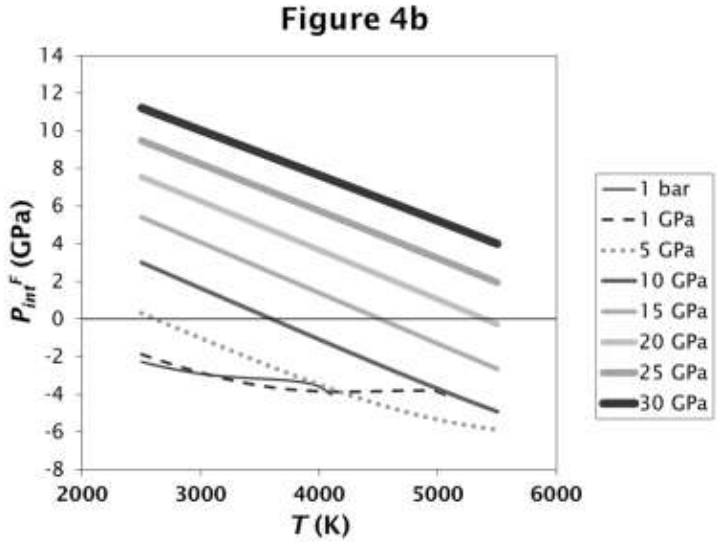

Figure 5

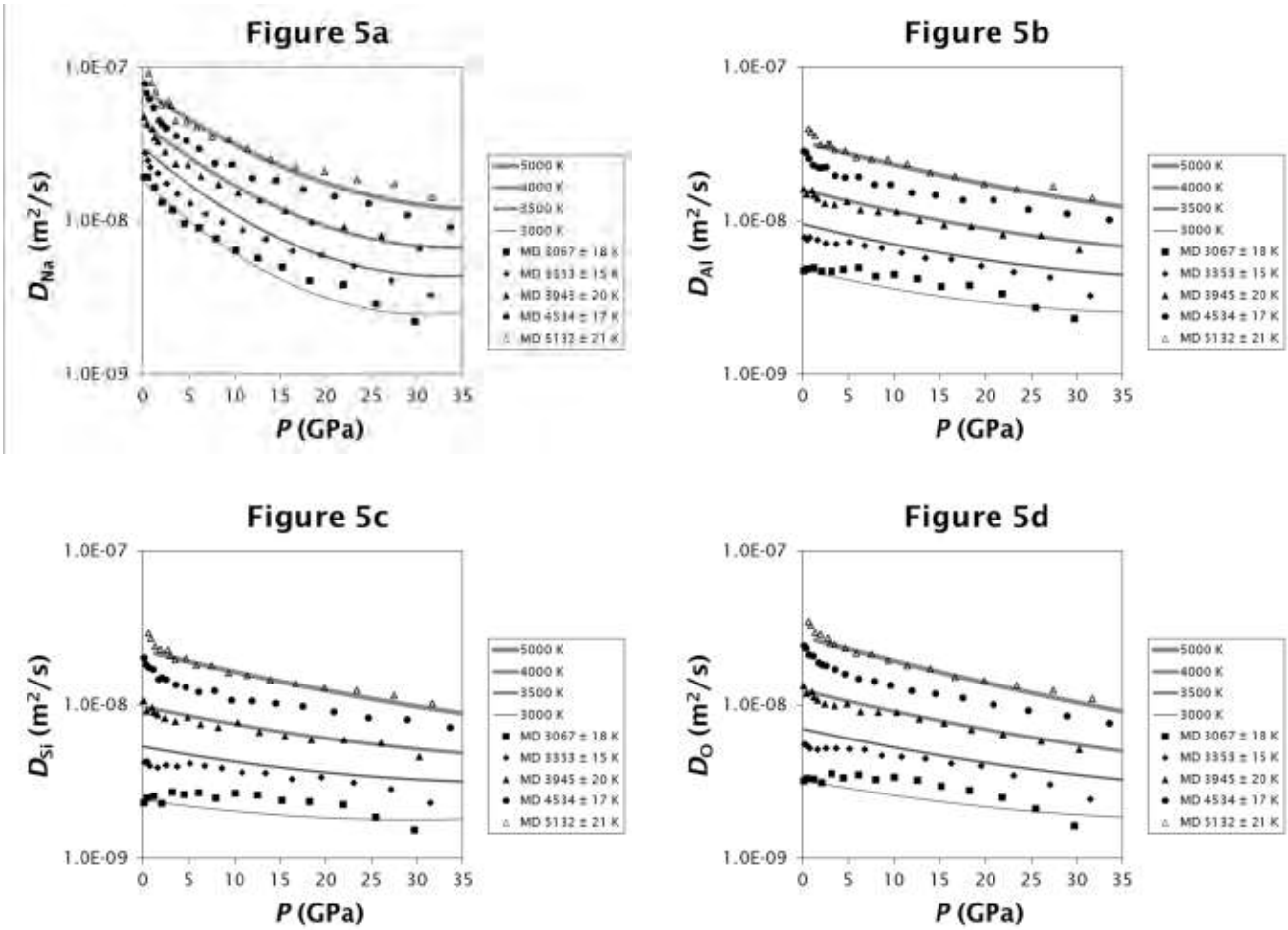

Figure 6

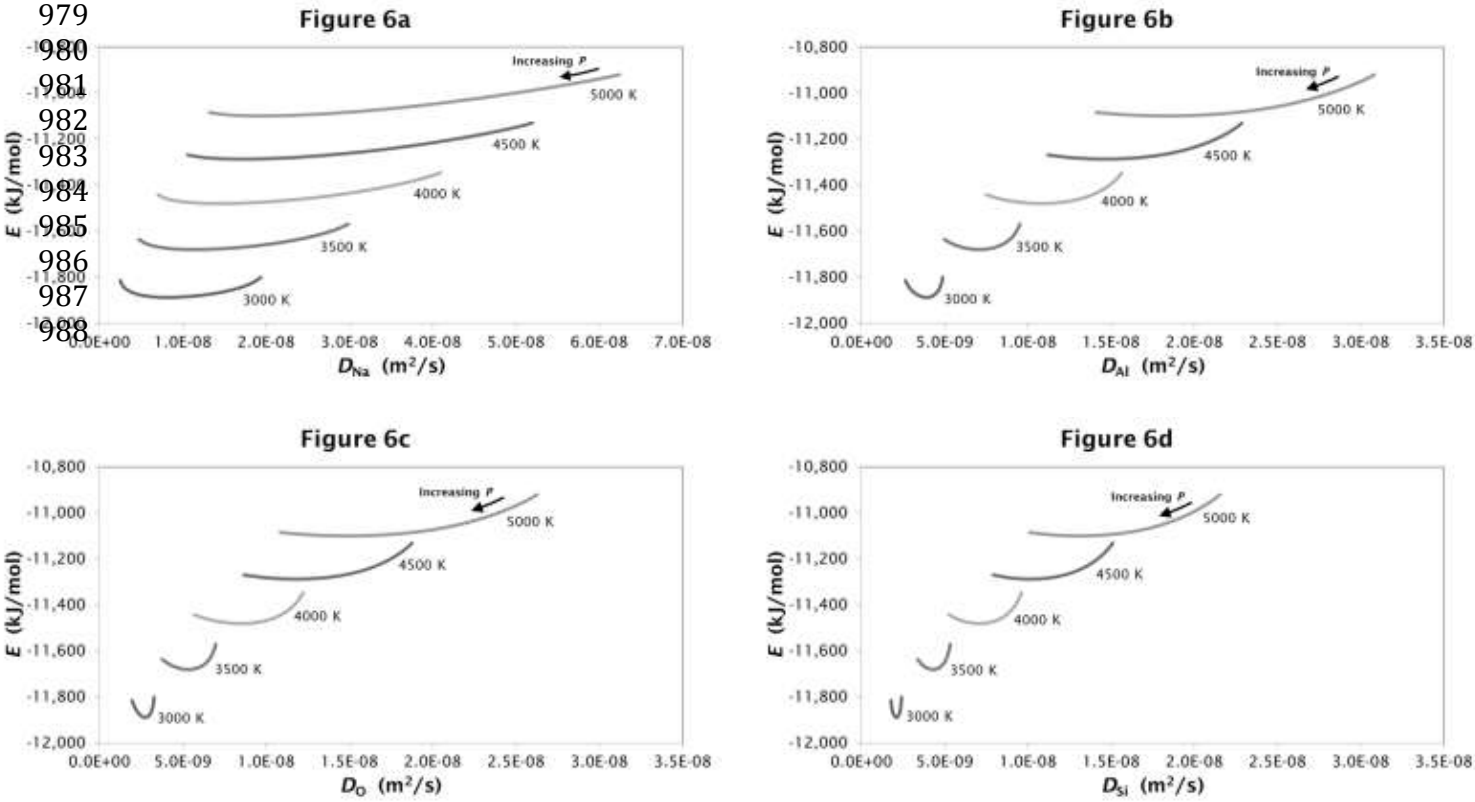

Figure 7

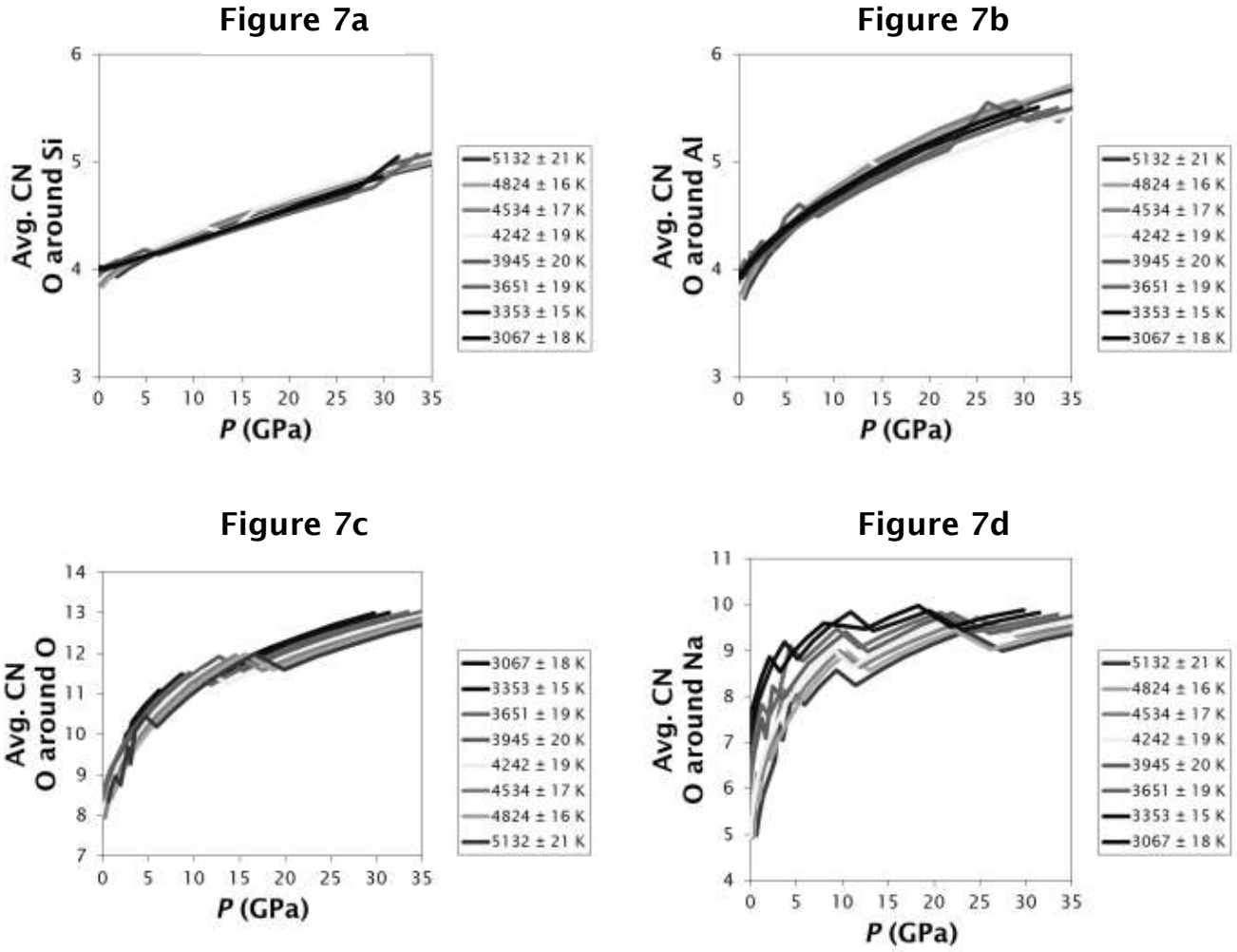

Figure 8

Figure 8a

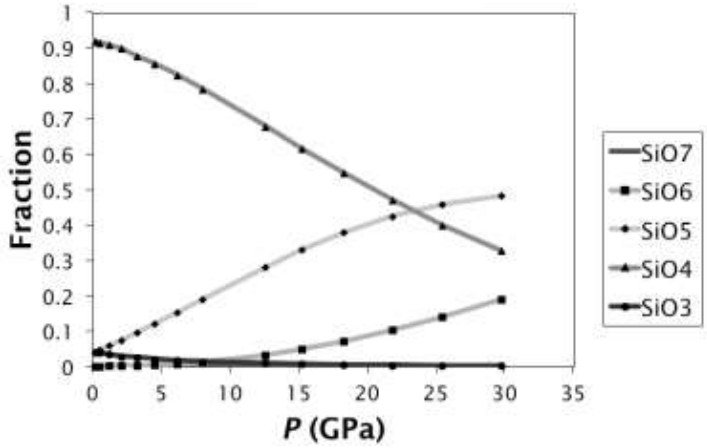

Figure 8b

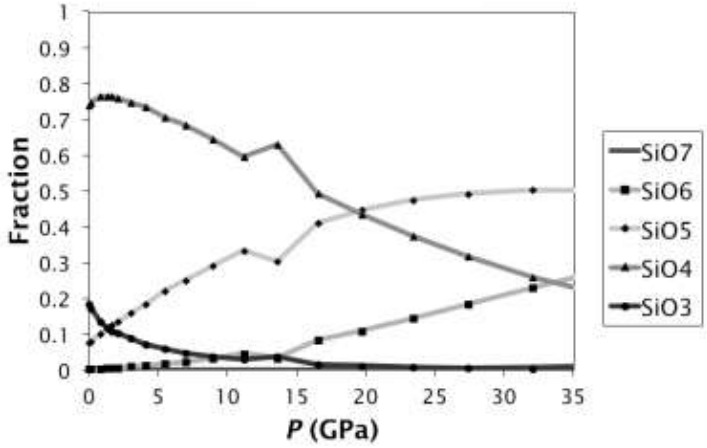

Figure 8c

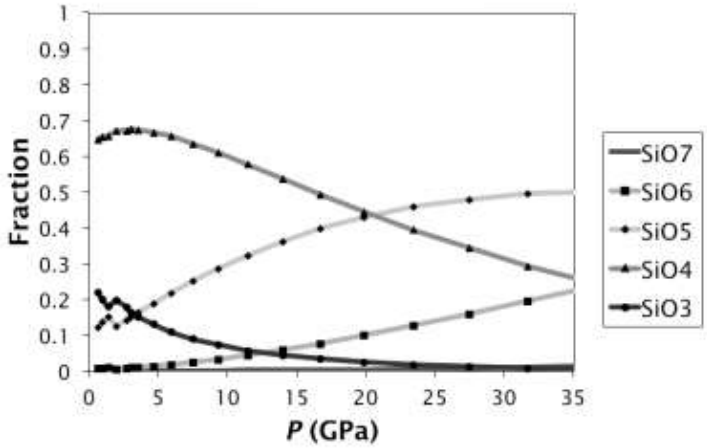

Figure 9

Figure 9a

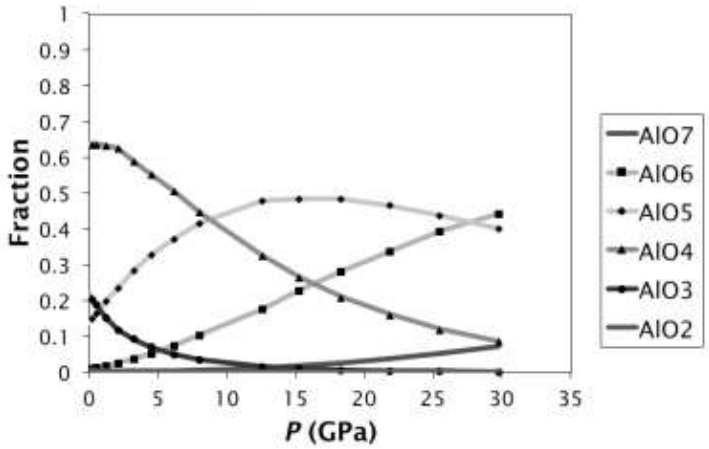

Figure 9b

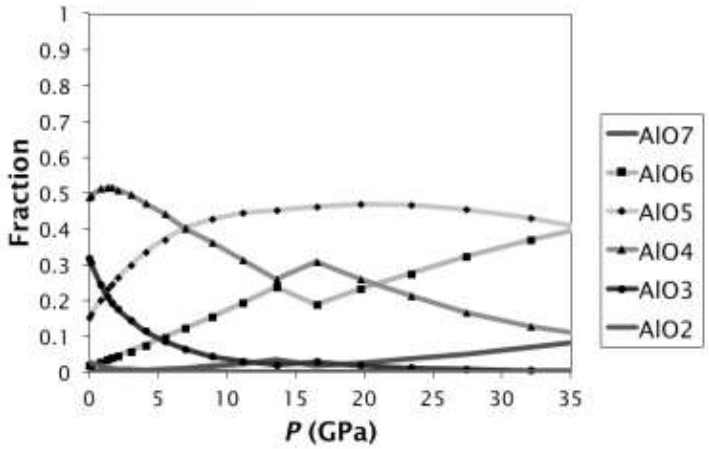

Figure 9c

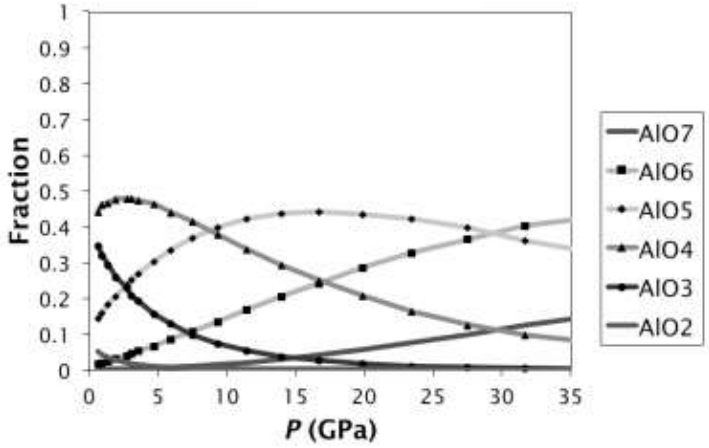

Figure 10

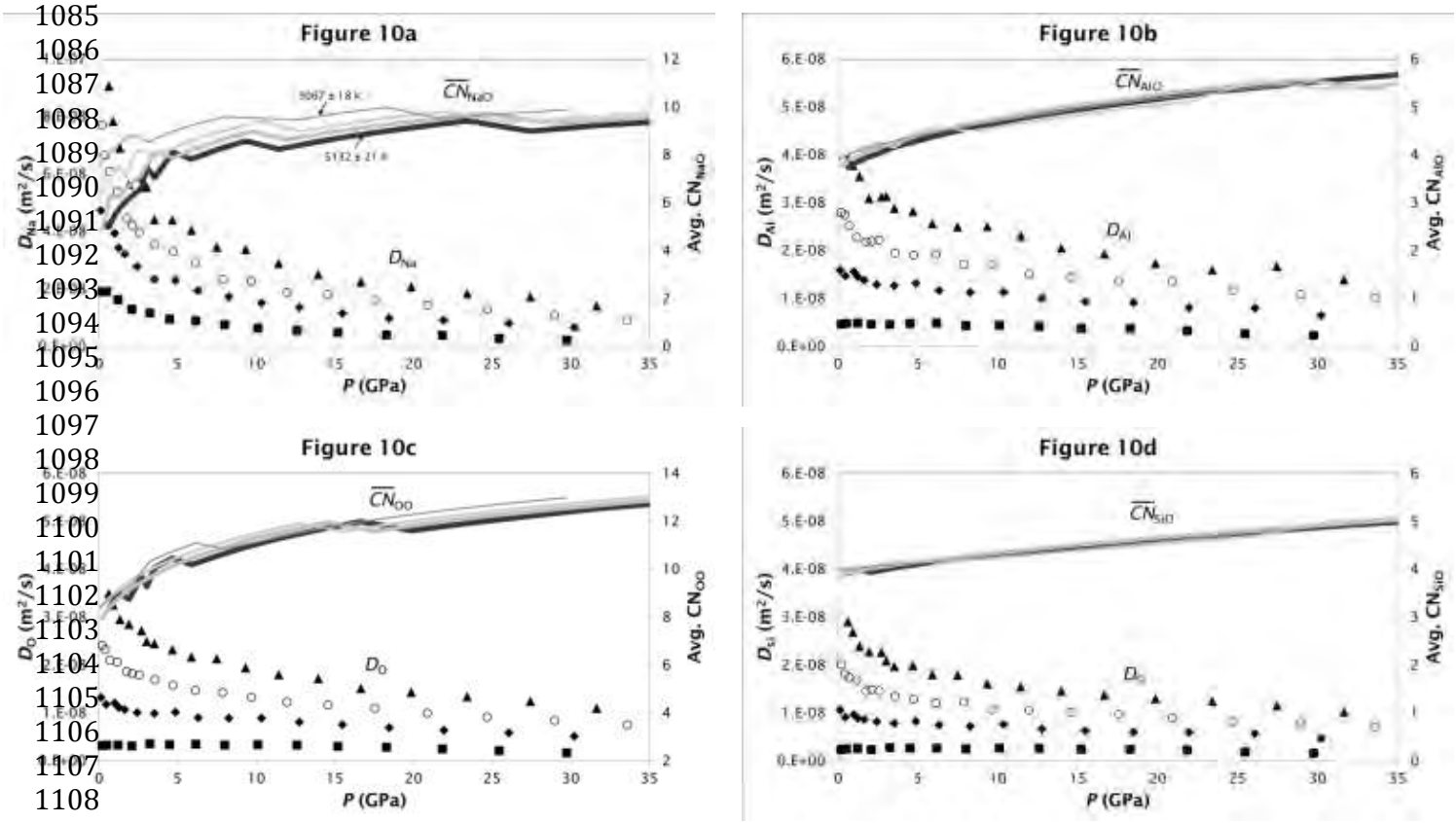

Figures for Appendices

Figure A1

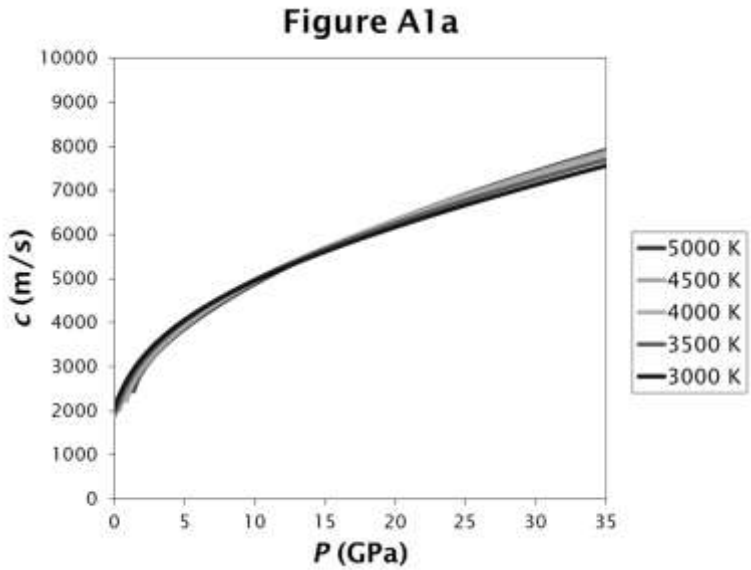

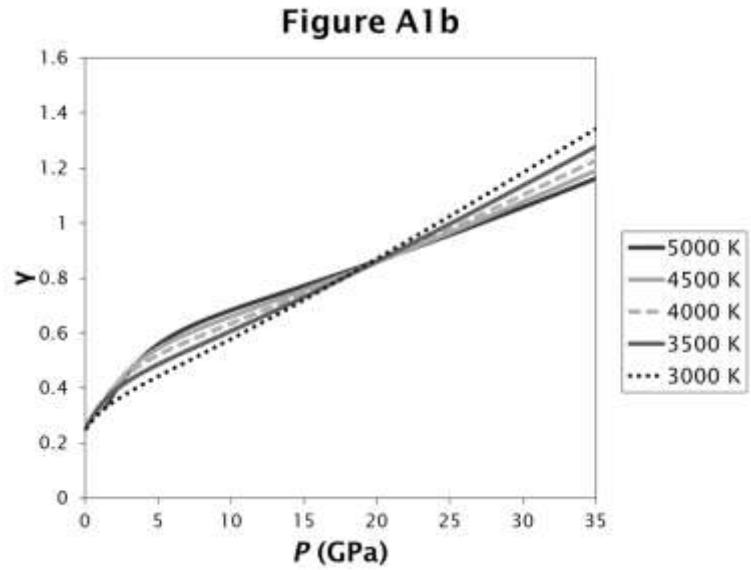

Figure A2